Optimization of CMOS MEMS Microwave Power Sensors

Veljko Milanović, Matthew Hopcroft, Christian A. Zincke, Michael Gaitan, and Mona E. Zaghloul

***Abstract* - Micromachined power sensors with operation up to 50 GHz were recently achieved in CMOS technology [1]. To improve their sensitivity and signal-to-noise ratio, while maintaining microwave performance, several design parameters must be considered, such as the number and placement of thermocouples. This paper presents experimental and analytical thermal characterization of the sensors, which provides insight into the proper adjustment of the layout parameters. Experimental results were obtained by indirect measurements of the sensor temperature distribution under various applied power conditions. A simple and approximate model was developed, and adjusted based on experimental results, which was then used to show the effects of the variations in layout parameters on the overall device sensitivity. The model includes thermoelectric Peltier and Thomson effects.**

I. Introduction

Thermocouple-based power sensors have been one of the most widely used tools for microwave power detection [2]. These sensors employ a simple principle of conversion of electric power to thermal power, which is then indirectly measured. We have recently developed a class of thermoconverters for broadband microwave power measurement up to 50 GHz [1],[3],[4] that are monolithically integrated in standard CMOS process by introducing novel post-processing micromachining methodology [1],[5].

In past IC implementations of thermoelectric sensors using micromachining techniques, the main design emphasis was to obtain as high sensitivity as possible [6],[7]. In our work the main objective was to attain good broadband microwave matching. This comes at the cost of lowered sensitivity, since the numerous thermocouples in very close proximity of the microwave termination resistor affect the sensor's microwave matching performance. At the same time, the necessary ground planes act as heat sinks and substantially decrease devices' thermal efficiency.

It is still possible to attain higher sensitivity by clever layout of the thermocouples, and proper adjustment of parameters such as: number of thermocouples, their suspended length, their proximity to the termination resistor, their lateral position with respect to the resistors' temperature distributions, etc. A tool is therefore needed for the optimization of the sensors that would predict overall device sensitivity and signal-to-noise ratio for a variety of layouts.

In this work, we report on the results of both experimental and analytical thermal characterization of the micromachined microwave power sensors, which provides insight into the proper adjustment of the above parameters to optimize device sensitivity. Experimental results were obtained by indirect measurements of the sensor temperature distribution under various applied power conditions. A simple and approximate model was developed, and adjusted based on experimental results, which was then used to show the effects of the variations in any of the above mentioned layout parameters on the overall device sensitivity.

The combined results present a very useful tool for the design of such thermoelectric sensors, such that development time can be greatly reduced.

II. Fabrication and Measurement Setup

Devices were fabricated through the MOSIS service, in the *n*-well 2.0 μm CMOS process. Subsequently, hybrid silicon micromachining methodology, described in detail in [5], was used to remove bulk silicon substrate beneath the high-frequency coplanar waveguides, microwave terminations, and hot thermocouple junctions. An example of a fully fabricated device is shown in Fig. 1.

Thermal measurements of actual devices were performed using a thermal imaging microscope. Suspended power sensors were prepared as described above and packaged in 40-pin DIPs. The packages were mounted on a copper block and attached to the microscope stage. Heat sink paste was used to ensure good thermal connections between the package and the stage. Power was applied to the sensor using a variable voltage source. Both applied voltage and current were monitored to record exact input power during measurements.

The thermal imaging microscope records 2-D images of radiance in the infrared wavelength range. The temperature of the device is determined by comparing radiance images of the device at known temperatures with radiance images of the device under test. These images were exported and analyzed using a mathematical software package. A zero-input radiance image was used to align the thermal images with the actual devices.

III. SPICE Equivalent Circuit for Thermal Model

Following nomenclature is used in this section, in agreement to that used by Swart and Nathan [8].

- A Area (m^2)
- h Heat-transfer coefficient (W/m^2K)
- I Current (A)
- l Length (m)
- q Heat transfer/unit area (W/m^2)
- q' Heat transfer/unit volume (W/m^3)
- T Temperature (K or °C)
- t_{CR} Temperature coefficient (1/K)
- κ Thermal conductivity (W/mK)
- R_0 Resistance at room temperature

The methodology for modeling of conduction and free convection used here was first introduced by Swart and Nathan in [8]. In their work, the thermal conduction, radiation, and convection equations [9] are translated into equivalent circuit elements and subsequently solved using SPICE. Heat flow is represented as current, temperature as voltage, and heat power as electrical power. Our analysis in this work is simplified from [8] in the following ways. In the convection model, only natural convection is of interest, and all convective losses are

V. Milanović is with the Berkeley Sensor and Actuator Center, University of California at Berkeley, 497 Cory Hall, Berkeley, CA 94720-1770: veljko@bsac.eecs.berkeley.edu.

M. Hopcroft, C. A. Zincke, and M. E. Zaghloul are with the Department of Electrical Engineering and Computer Science, The George Washington University, Washington, DC. M. Gaitan is with the Semiconductor Electronics Div., Natl. Inst. of Standards and Technology (NIST), Gaithersburg, MD.

The work was performed at NIST, and was partially supported by Space and Naval Research Sys. Ctr., RDT&E DIV, San Diego, CA.

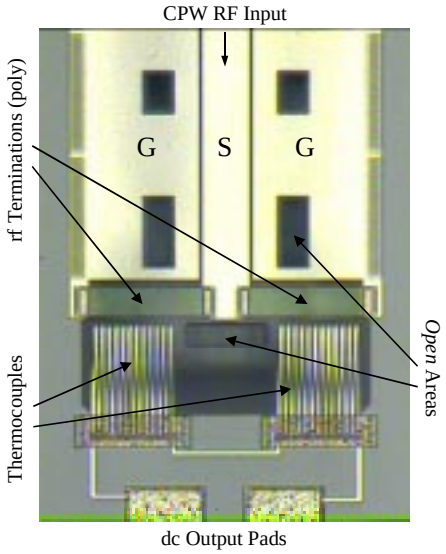

Figure 1. Microphotograph of the CMOS micromachined microwave power sensor.

lumped into one thermal resistance term. Another simplification is in the subdivision of the actual structure in a relatively small number of regions in a two-dimensional plane, as shown in Fig. 3, since we are more interested in observing optimization trends, rather than attempting to predict device performance very accurately. Finally, as an additional simplification, temperature dependence of thermal conductivity for the materials present, and radiation losses, are neglected. This is easily justified since the devices are specified to operate up to 10 mW maximum input power for which case maximum temperature on the device is < 100 °C, and therefore not much above room temperature.

Therefore, in the simulations of interest here, we are only interested in 2D steady state case conduction, and free convection. Steady state case conduction is given by the Poisson equation:

$$\nabla \cdot (\kappa \nabla T) = -q'. \tag{1}$$

Total heat transfer from a surface A due to free convection is given by:

$$q = hA(T_s - T_f), \tag{2}$$

where T_s is surface temperature and T_f is the free stream temperature in the case of forced convection, or simply ambient temperature.

The three-dimensional thermopile structure is treated as 2D in the layout plane, due to the fact that only air is present above and below the structure, and the convective losses in those directions can be combined into one resistive circuit element at each element in the plane. The 2D layout is further subdivided into smaller elements, each being one of four types as shown in Fig. 3. Since the modeling was not aimed at high accuracy, the subdivisions are relatively large, as shown in the figure. Each element is then represented as the equivalent circuit of Fig. 4, with particular values depending on the element type, and size. In general, the resistors in the figure are non-linear, and may depend on the temperature or other parameters. The current source in Fig. 4 is only applicable for resistive elements in the device structure where dissipated power generates heat, and may also have temperature and other dependence.

In accordance with Swart and Nathan [8], each of the circuit elements shown in Fig. 4, representing heat transfer, is

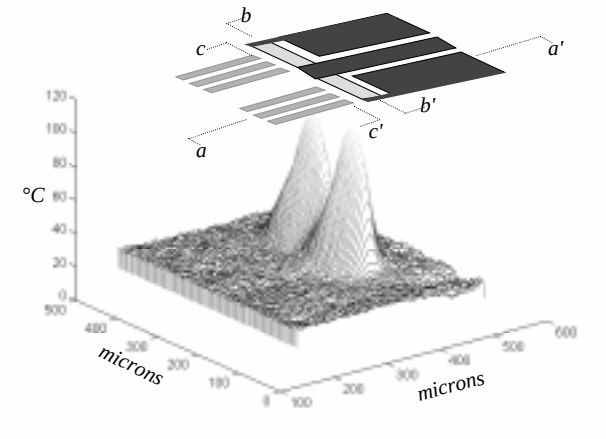

Figure 2. Measured temperature distribution at dc bias of 20 mW.

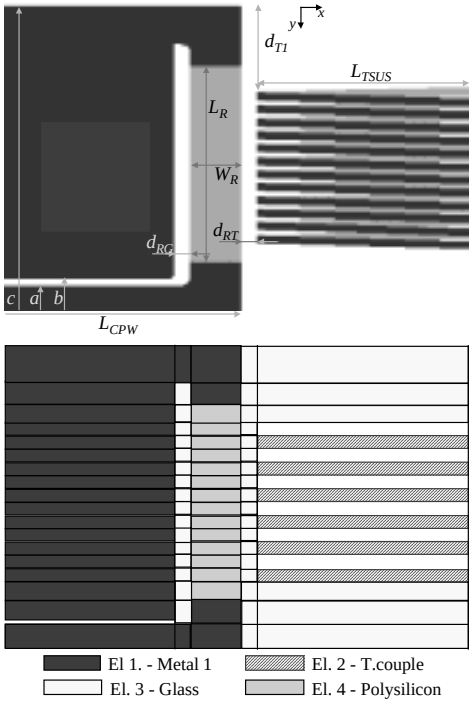

Figure 3. (Upper figure) Outline of half the thermopile (even symmetry), showing pertinent dimensions for optimization. (Lower figure) The corresponding four types of elements and subdivisions used in simulations.

described by a voltage-controlled current source (VCCS). The form used here is simply:

$$I = a_0 + a_1 V + a_2 V^2 + \ldots, \tag{3}$$

since it sufficiently describes the thermal resistances shown in the figure, and the temperature-dependent heat generation in polysilicon.

In the simple case where there is no variation in parameters due to change in temperature, the conductive transfer of (1) in 2D is simply represented as thermal resistance:

$$R_{th} = l/\kappa \cdot A, \tag{4}$$

where A is cross-sectional area of the element. This assigns the coefficients of the VCCS in (3) with $a_1 = \kappa A$, and $a_0 = 0$. This sets up the four conduction resistors R_1 and R_2 which differ from element to element by the κ and A. The convection resistor R_h

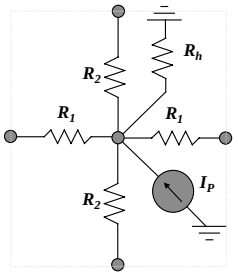

Figure 4. Equivalent electrical circuit representation of an element of Fig. 3, including convection, conduction and heat generation.

is also represented by a VCCS with $a_1=hA$ to implement (2), but here A is surface area. Joule heat generation, equal to power dissipation, could be modeled by a constant-current source. However, the input power to the resistive microwave termination is dissipated by the thin-film polysilicon heater, whose resistance is a strong function of temperature. Due to this strong temperature dependence, the input power is implemented as:

$$I_P(T) = I^2 R_0 + I^2 R_0 \cdot t_{CR}(T - T_0), \tag{5}$$

which sets up $a_0=I^2R_0$ and $a_1=t_{CR}\, I^2R_0$.

IV. Simulation Setup, Results and Discussion

Simulations were set up by forcing constant current excitation 2I at power sensor input, therefore nominally forcing input power $(2I)^2R_{term}$. The even symmetry condition, as shown in Fig. 3, was set up by doubling values of resistors R_1 in the bottom row, and cutting off lower resistors R_2 in that same row. The constant input current I was therefore forced into the resistor, which enters (3). After the network of VCCSs is created and simulated in SPICE, the resulting node voltages are treated as temperatures, and the heater temperatures are fed back to obtain the adjusted termination resistance:

$$R_{term\_adj} = R_0 \sum_i \left(1 + \alpha_{poly} \cdot (T_i - T_0)\right), \tag{6}$$

since each *i-th* subdivision has increased resistance. Hence, the actual power dissipated in the termination resistors is:

$$P_{diss} = (2I)^2 \cdot R_{term\_adj}. \tag{7}$$

The thermopile output voltage is a sum of temperature differences of all hot and cold junctions with Seebeck coefficient as weighing function:

$$V_{out} = \alpha_{tc} \cdot \sum_i^{N_t} (T_h - T_0), \tag{8}$$

and finally, sensitivity is simply $S = V_{out} / P_{diss}\,[V/W]$.

After running the SPICE simulations, we identified the nodes that belong to the center cut through the polysilicon resistors (b-b' in Fig. 3), as well as the nodes at the hot thermocouple junctions (c-c' in Fig. 3), since those two sets produce most of the needed information for analysis. The modeled results were compared with measured ones. The comparison of model and simulations for the b-b' cut through the sensor structure of Fig. 2, is shown in Fig. 5. In the figure, it can be seen that the modeled temperature distribution with convection included closely resembles the measured distribution. The main points of matching are the nearly equal top values of temperature, and the distribution toward the middle of the signal conductor, where temperature remains well above the substrate temperature, but is significantly colder than the middle of the heater. On the other hand, due to the limited resolution of the

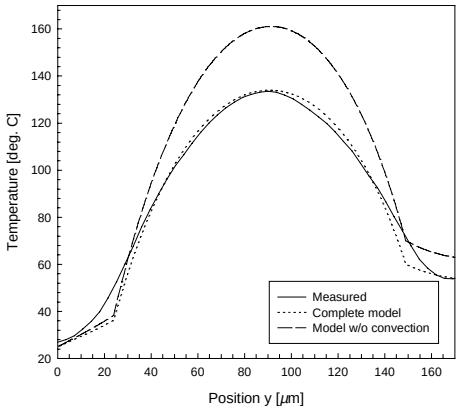

Figure 5. Compared results of temperature distribution across one termination resistor arm for model and measurement. With convection included in model, it matches measurements well.

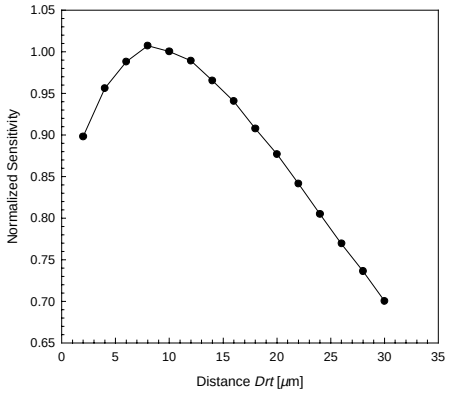

Figure 6. Computed sensitivity as a function of the distance of hot thermocouple junctions from the resistor.

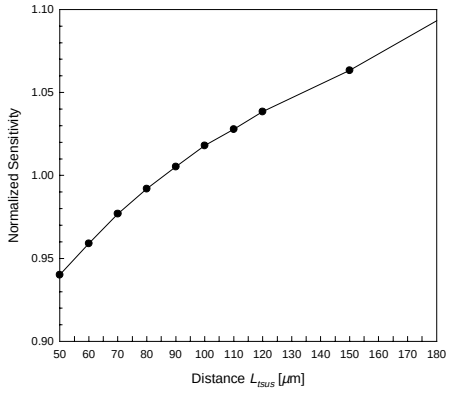

Figure 7. Computed sensitivity as a function of the suspended length of the thermocouples (24 thermocouples).

thermal microscope, the measured temperature distribution shows slowly decreasing tails and does not have sharp features the model predicts at material boundaries. This is accompanied by the slightly different shape toward the peak temperature which we attributed to "parasitic" Peltier and Thomson effects.

As mentioned earlier, essential parts in the optimization of the sensor are the heat sinking effect of each thermocouples, and the signal-to-noise ratio resulting from thermocouple series resistance. Firstly, we were interested in the effect of thermopile distance from the resistor. We were already aware of at least two possible detriments of very close proximity. One has to do with the broadband match of the termination which looks like a 50 Ω

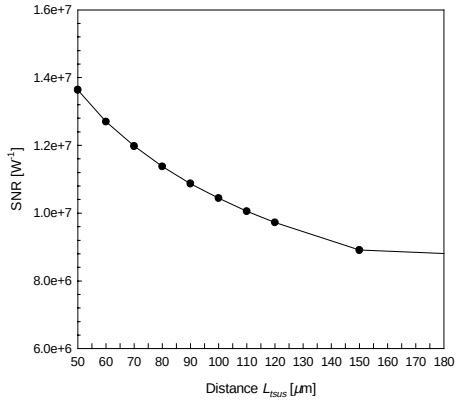

Figure 8. Computed SNR for 24 thermocouples in series as a function of suspended thermocouple length L_{tsus}.

resistance to a microwave source in a very wide range of frequencies. This is in part due to approximate 100 Ω characteristic impedance (as well as 100 Ω resistance) in each arm of the tee, as described in [1],[3]. That proper capacitance is established between the resistor in each tee and the adjacent ground plane. Hence, moving the thermopile too closely would increase the capacitance in the arms and *detune* the termination from its best match. The second possible detriment was expected to be due to increase of thermal conductance with closer thermopile, and therefore decrease of thermal efficiency.

The results in Fig. 6 are plotted on a normalized scale with unity sensitivity for D_{rt} of 12 μm, as in the fabricated sensor. As the figure shows, there is an actual *optimum* distance for the thermopile which trades off the thermal phenomena, and would hopefully be compatible with electromagnetic requirements.

Another parameter is the suspended length of the thermopile. For increased L_{tsus}, the thermal conductance of the thermopile decreases, and the sensor becomes more thermally efficient. This effect is shown in Figure 7. The trade-off for the length is the signal-to-noise ratio. The effect of the increase of thermopile resistance lowers the SNR, defined as $SNR = S/V_n$ $[W^{-1}]$, where $V_n=(4kTR_{tp}B)^{1/2}$. The resistance in the thermocouples is dominated by poly resistance, which for our sensors was roughly 6.8 Ω/μm length. Since a total of 24 thermocouples in series was utilized, the total resistance entering into the calculation of SNR is $163.2\ L_{tsus}$ Ω. The computed SNR is shown in Figure 8. For the structure shown in Figure 1, the length is 85 μm, for which the true computed 1 Hz bandwidth SNR at minimum input power of 1 μW reads 11.3.

We also performed a parametric variation on the number of thermocouples. The number was varied from 1 to 12 for ½ section, and sensitivity plotted in Figure 9 normalized with respect to the fabricated 24-thermocouple sensor. At first in the plot, additional thermocouples significantly increase the sensitivity in an almost linear fashion. This trend changes at 14 thermocouples after which improvement is much slower. Nevertheless, the sensitivity continually increases, even though additional thermocouples increase total thermal conductance. The overall performance effect is, however, not all positive. Namely, the resistance increase with each additional pair of thermocouples significantly decreases SNR, as shown in Fig. 10. Because the SNR plot was normalized to sensitivity, the plot shows that there is an optimum number of thermocouples for Sensor 1, 14 thermocouples with SNR over $1.2x10^7$.

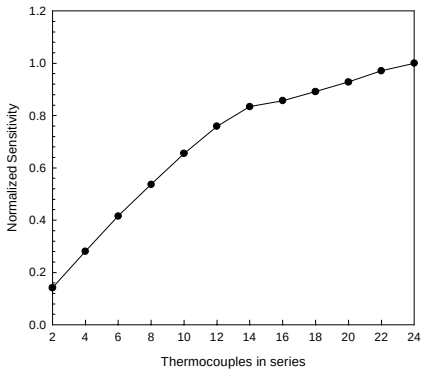

Figure 9. Computed sensitivity as a function of the number of thermocouples tightly distributed about the center of the resistor.

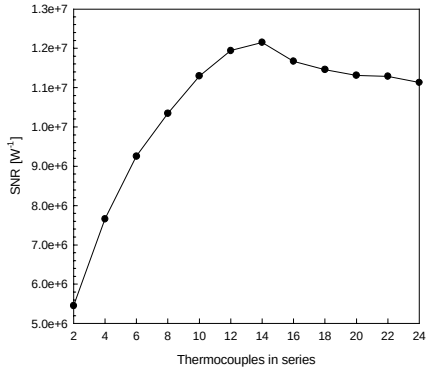

Figure 10. Computed SNR as a function of the number of thermocouples.

V. Conclusions

The presented model, verified by experimental results is shown to be very useful in the optimization of the microwave power sensor. The results also show a number of phenomena that take place in the operation of the sensor and affect its sensitivity, peak temperature, resistor drift, etc.

References

[1] V. Milanović, *Micromachined Broadband Thermocouple Microwave Power Sensors in CMOS Technology*, D.Sc. Dissertation, The George Washington University, Jan. 1999.

[2] Hewlett Packard Co., "Fundamentals of RF and Microwave Power Measurement," Appl. Note AN 64-1, Jun. 1978.

[3] V. Milanović, M. Gaitan, E. Bowen, N. Tea, and M. Zaghloul, "Thermoelectric Power Sensor for Microwave Applications in CMOS Technology," *IEEE Electron Device Lett.*, vol. 18, pp. 450-452, Sep. 1997.

[4] V. Milanović, M. Gaitan, M. Zaghloul, "Micromachined Thermocouple Microwave Detector by Commercial CMOS Fabrications," *IEEE Tran. on Microwave Theory and Tech.*, vol. 46, no. 5, May 1998.

[5] N. H. Tea, V. Milanović, C. Zincke, J. S. Suehle, M. Gaitan, M. Zaghloul, and J. Geist. "Hybrid Post-processing Etching for CMOS-compatible MEMS," *IEEE Journal of MEMS*, Feb. 1997.

[6] D. Jaeggi and H. Baltes, "Thermoelectric AC Power Sensor by CMOS Technology," IEEE Electron Device Letters, vol. 13, no. 7, Jul. 1992.

[7] M. Gaitan, J. Kinard, and D. X. Huang, "Performance of Commercial CMOS Foundry-Compatible Multijunction Thermal Converters," *Transducers'93 Conf., Yokohama, Japan*, Jun. 1993.

[8] N. R. Swart and A. Nathan, "Flow-rate microsensor modelling and optimization using SPICE," *Sensors and Actuators A*, vol. 34, pp. 109-122, 1992.

[9] H. B. Callen, *Thermodynamics and an Introduction to Thermostatics*, 2nd ed., John Wiley & Sons, New York, 1985.